Neoproterozoic (750–711 Ma) Tectonics of the South Qinling Belt, Central China: New Insights from Geochemical, Zircon U-Pb Geochronological, and Sr-Nd Isotopic Data from the Niushan Complex

WANG Shuo[1], LIU Yunhua[1,*], YANG Benzhao[2], TAN Le[2], LI Xiaoyan[3] and DENG Nan[4]

[1] *School of Earth Sciences and Resources, Chang'an University, Xi'an 710054, China*
[2] *Geological Team No. 1 of Shaanxi Bureau of Geology and Mineral Resources, Ankang, Shannxi 725000, China*
[3] *Longshou Mine of Jinchuan Group Co., Ltd, Jinchang, Gansu 737100, China*
[4] *Xi'an Mineral Resources Survey Center, China Geological Survey, Xi'an 710100, China*

Abstract: The Xiejiaba and Fuqiangbei plutons form part of the newly identified Neoproterozoic Niushan complex, which is located in the southern South Qinling belt (SQB). The plutons are compositionally similar, were emplaced at 750–711 Ma, and provide insights into Neoproterozoic tectonism within the South Qinling belt. The Xiejiaba pluton contains diorite, quartz diorite, granodiorite, and granite phases, all of which are sub-alkaline and have variable major element compositions with negative correlations between SiO_2 and MgO, TFe_2O_3, Al_2O_3, CaO, TiO_2 and P_2O_5. These rocks are enriched in light rare earth elements (LREEs) and large ion lithophile elements (LILEs) and have negative Nb, Ta, P and Ti anomalies, all of which are indicative of arc-type magmatism. The Fuqiangbei pluton contains granitoids that are compositionally similar to the rocks in the Xiejiaba pluton. Samples from these plutons have similar $\varepsilon_{Nd}(t)$ values (1.24–5.99) but very variable $(^{87}Sr/^{86}Sr)_i$ values (0.7010–0.7054). Combining these data with the geochemical data for these rocks suggests that the magmas that formed the Niushan complex were derived from the crust–mantle boundary. This, combined with the results of previous research, suggests that the transition from low pressure-low temperature to low pressure-high temperature conditions within a subduction zone caused melting during a period of late subduction and backarc extension. This constrain the timing of subduction within the South Qinling belt and the northern Yangtze Block (YB) to 750–711 Ma, with this Neoproterozoic subduction associated with an ocean to the north overprinting an existing continental rift-type tectonic setting within the northern margin of the Yangtze Block and the South Qinling belt.

Key words: geochronology, geochemistry, magmatism, tectonics, Precambrian, South Qinling

Citation: Wang et al., 2023. Neoproterozoic (750–711 Ma) Tectonics of the South Qinling Belt, Central China: New Insights from Geochemical, Zircon U-Pb Geochronological, and Sr-Nd Isotopic Data from the Niushan Complex. Acta Geologica Sinica (English Edition), 97(1): 106–121. DOI: 10.1111/1755-6724.14926

1 Introduction

The Qinling Orogen of central China (Fig. 1a) links the Kunlun–Qilian Orogen to the west with the Sulu–Dabie Orogen to the east, and represents a composite orogenic belt formed by the Triassic collision between the North (NCC) and South (SCC) China cratons. The main orogen is divided into the North Qinling belt (NQB) and South Qinling belt (SQB) (Zhang et al., 2001; Dong et al., 2011a, b, c; Wu and Zheng, 2013). Recent research on the Neoproterozoic tectonic evolution of the Yangtze Block (YB), including the SQB, has focused on the western and southern margins (Wan et al., 2019; Wang et al., 2019a; Yao et al., 2019; Wei and Zhao, 2020; Zhang et al., 2020). However, the Neoproterozoic tectonic history of the northern margin of the YB, including the SQB, remains controversial. Some research suggests that regional Neoproterozoic tectonic-magmatic events within the SQB and the northern margin of the YB have global significance and are associated with the amalgamation and break-up of the Rodinia supercontinent. The genesis and tectonic setting of the igneous rocks in these areas remain uncertain, with plume-rift, intracontinental rift, and slab-arc type models all being suggested. In addition, the Neoproterozoic position of the SCC, including the YB and the SQB, within the Rodina supercontinent also remains uncertain. For example, Li et al. (1995, 1999) suggested that the SCC was located in central Rodinia, forming a link between Australia–East Antarctica and Laurentia. This suggestion implies that the Neoproterozoic magmatism in the SCC formed as a result of mantle plume activity and/or intracontinental rifting (Li H K et al., 2003; Li Z X et al., 2003; Wang et al., 2009). However, other models place the YB within the margins of the Rodinia supercontinent, suggesting that the Neoproterozoic magmatism was associated with subduction and arc-type magmatism along the western, northern, and southeastern YB margins (Xiang et al., 2015; Dong et al., 2017; Zhang et al., 2018; Ao et al., 2019; Wang R R et al.,

* Corresponding author. E-mail: zyyhliu@chd.edu.cn

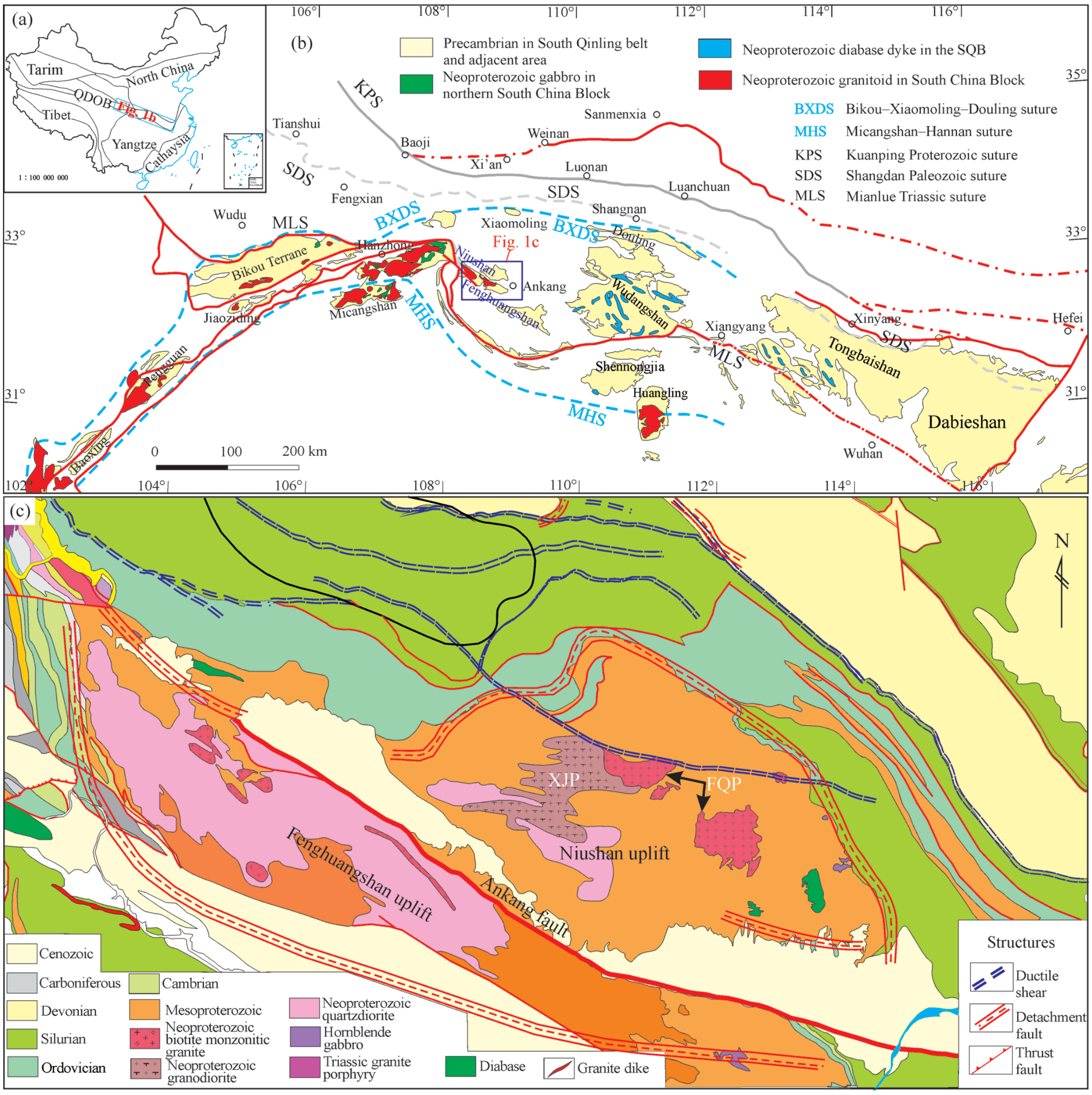

Fig. 1. (a) Map showing the location of the Qinling orogen and other major blocks within China; (b) simplified tectonic maps of the South Qinling belt and adjacent areas (modified after Dong and Santosh, 2016) showing the tectonic subdivision, distribution of Precambrian rocks, and the ages of Neoproterozoic igneous rocks; (c) simplified geological map of the study area.
China basemap after China National Bureau of Surveying and Mapping Geographical Information.

2019; Wang Y J et al., 2019; Nie et al., 2019).

This study presents new zircon U-Pb geochronological, petrological, geochemical, and Sr-Nd isotopic data for samples from the Neoproterozoic Niushan complex, which was originally thought to have formed during the Triassic. Combining these new data with the results of previous research allows us to further constrain the Neoproterozoic tectonic setting and geodynamic processes recorded within the SQB and will provide insights into the position of the SCC within the Rodina supercontinent.

2 Geological Setting and Sampling

The SQB is located between the Shangdan and Mianlue sutures (Dong et al., 2014) (Fig. 1b), forms the northern part of the YB, and is separated from the YB by the Mianlue suture in the early Paleozoic. Previous geological, geochemical, and geochronological research in this area indicates that the SQB broke away from the YB as a discrete microcontinent during the Paleozoic opening of the Mianlue Ocean (Zhang et al., 1995, 2001; Li et al., 1996; Dong et al., 1999, 2011c) before being accreted to the NQB and the NCC during the Triassic. This hypothesis is consistent with the presence of similar latest Neoproterozoic and lower Paleozoic sedimentary successions within the SQB and YB (Zhang et al., 2001). In addition, the collision of the SQB microblock with the northern continental margin of the YB records the late Paleozoic–Early Triassic closure of the intervening Paleo-Tethys Ocean.

The SQB is dominated by thin-skinned structures that include a southward-curving fold-and-thrust belt consisting of Precambrian basement material and overlying Phanerozoic sedimentary rocks (Zhang et al., 2001; Dong et al., 2013). The study area is located within the southern SQB (Fig. 1c) and hosts middle–late Proterozoic basement material that was metamorphosed under greenschist to

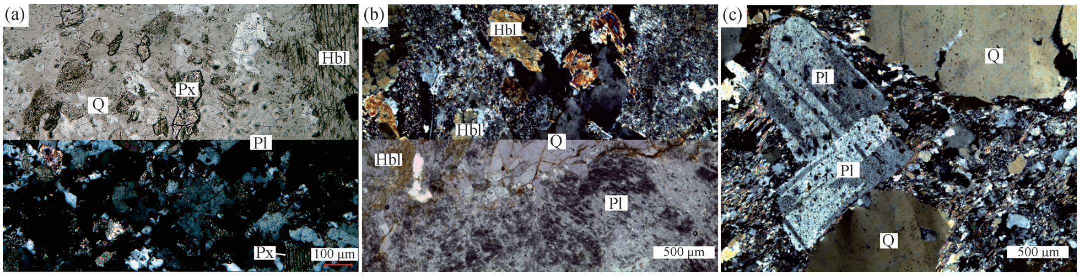

Fig. 2. Photomicrographs of intrusive rocks from the Niushan complex: diorite (a) and granodiorite (b) from the Xiejiaba pluton (XJP); (c) granite porphyry from the Fuqiangbei pluton (FQP).
Hbl–hornblende; Pl–plagioclase; Q–quartz; Px–pyroxene.

lower amphibolite facies conditions. All of the Precambrian basement in this region was originally covered by sedimentary strata, including uppermost Neoproterozoic clastic and carbonate rocks. The Neoproterozoic Yaolinghe Group contains greenschist facies metamorphosed basalt and basaltic andesite with minor rhyolite and dacite, although only small outcrops of this group are exposed in the study area. The southwestern part of the study area contains carbonaceous slate and conglomerate-bearing sandy limestone of the Ordovician Donghe Formation and carbonaceous slate and interbedded volcanic rocks of the Late Ordovician–Early Silurian Banjiuguan Formation. Greenschist facies metamorphosed volcanic-sedimentary rocks of the Silurian Meiziya Formation are also widely distributed in the study area with lesser amounts of the late Paleozoic Shijiagou, Dafenggou, and Gudaoling formations.

Multi-stage WNW–ESE- or approximately E–W-trending ductile shear zones are distributed in the study area, and multiple decollement structures that formed during the multi-stage Niushan–Fenghuangshan uplift event are found. These ductile shear zones surround the Niushan–Fenghuangshan uplift and with the decollements are cross-cut by the Triassic Ankang fault. Middle–late Proterozoic and Early Jurassic intermediate–felsic intrusions are also distributed in the study area. Triassic granitoids and late Paleozoic metamorphic rocks have also been identified within the SQB and are thought to have formed during the collision between the NCC and the YB (Sun et al., 2002; Qin et al., 2007). The Niushan complex was emplaced into Neoproterozoic country rocks and was originally thought to have formed during the Triassic. However, our zircon U-Pb dating of the complex indicates that it formed during the Neoproterozoic (750–711 Ma). This new age range means that the complex can provide insights into the Neoproterozoic tectonic evolution of the SQB and the northern margin of the YB.

The Niushan complex is located within the southern SQB and intruded into the Mesoproterozoic Yangping Formation. The complex is divided into the Xiejiaba (XJP) and Fuqiangbei (FQP) plutons, where the XJP contains a differentiation-associated sequence of diorite, quartz diorite, granodiorite and granite phases and the FQP consists of a single granitoid phase. The diorites within the XJP are medium- to coarse-grained, massive, and contain hornblende and plagioclase with minor amounts of pyroxene (Fig. 2a). The diorite consists of subhedral plagioclase crystals (50–55 vol%) up to 6.0 mm across, and lozenge-shaped (2.0–5.0 mm) hornblende with two cleavages (~30 vol%). The quartz diorite and granodiorite are fine- to coarse-grained and massive and contain plagioclase, quartz, and hornblende (Fig. 2b). Subhedral to anhedral plagioclase (0.1–0.5 mm in diameter) form 40–50 vol% of the quartz diorite and granodiorite phases with interstitial spaces filled by subhedral hornblende, forming 15–30 vol% of these units. The granite is medium- to coarse-grained, porphyritic (Fig. 2c), and massive and contains subhedral plagioclase phenocrysts (40–50 vol%) along with matrix-hosted subhedral-anhedral and wormlike quartz (45 vol%) and minor amounts of sericite (5 vol%).

3 Analytical Methods

Zircons were separated by handpicking with high quality zircons free of fractures chosen for analysis. These zircons were mounted and polished to obtain a clean and flat surface before cleaning in an acid bath prior to analysis by laser ablation-inductively coupled plasma-mass spectrometry (LA-ICP-MS) at the State Key Laboratory of Continental Dynamics, Northwest University, Xi'an, China. Prior to LA-ICP-MS, internal zircon structures were imaged using cathodoluminescence (CL). The single zircon U-Pb isotope analysis undertaken during this study used a Perkin Elmer/SCIEX ELAN 6100 ICP-MS instrument coupled with a dynamic reaction cell (DRC) and employing a 30 mm-diameter laser spot. An NIST610 standard silicate glass was used for instrument optimization to obtain maximum signal intensities (^{238}U signal intensity is 1000–1600 cps/ppm) and low oxide production (ThO/Th < 1%). Ratios of ^{207}Pb/^{206}Pb, ^{206}Pb/^{238}U, ^{237}Pb/^{235}U, and ^{208}Pb/^{232}Th were calculated using the GLITTER 4.0 software package and corrected for instrumental mass bias and depth-dependent elemental and isotopic fractionation using a 91500 zircon as an external standard. The concentrations of U, Th and Pb were calibrated using ^{29}Si as an internal standard and the NIST SRM 610 standard for external standardization. Dates were calculated using ISOPLOT v. 3.0 (Ludwig, 2003) and common Pb corrections were undertaken using the approach of Andersen (2002). Age uncertainties are quoted at the 95% confidence level.

Whole-rock major and trace element compositions were determined by X-ray fluorescence (XRF) and ICP-MS, respectively, at the MOE Key Laboratory of Western China's Mineral Resources and Geological Engineering, Chang'an University, Xi'an, China. Rock powders were fused to make glass disks for XRF analysis and were digested in acid within steel-jacketed Teflon ‘bombs’ to generate solutions for ICP-MS analysis. The analytical uncertainties are ~5% for major elements and ~10% for trace elements.

Whole-rock Sr-Nd isotopic compositions were determined using thermal ionization mass spectrometry (TIMS) employing an IsoProbe-T instrument at the Geological Research Institute of Nuclear Industry, Beijing, China. Total procedural blanks for Sr and Nd were <200 and <100 pg, respectively. Analysis of the La Jolla Nd and 195 SRM987 Sr standards yielded values of $^{143}Nd/^{144}Nd$ = 0.511864 ± 0.000003 (2s, n = 6) and $^{87}Sr/^{86}Sr$ = 0.710236 ± 0.000007 (2s, n = 6), respectively.

4 Analytical Results

4.1 Zircon U-Pb results

Diorite (XJ-01) and granite (FQP-01) samples from the Niushan complex were dated using the zircon U-Pb approach, with the results of this analysis given in Supp. Table 1. All of the zircons from these samples are crystalline and have length/width ratios of 1.5:1–3:1. The crystals are light yellow to colorless and have clear magmatic oscillatory zoning visible during CL imaging (Fig. 3), suggesting that they have a magmatic origin. Zircons from diorite sample XJ-01 and granite sample FQP-01 have high Th/U ratios of 0.88–3.33 and 1.04–12.45, respectively, which are consistent with a magmatic (0.2–1.0) rather than metamorphic (<0.1) origin, further supporting a magmatic origin for these zircons (Williams and Claesson, 1987; Schiotte et al., 1988; Kinny et al., 1990).

A total of 30 individual analyses of zircons from diorite sample XJ-01 yield 16 concordant data points that plot on or near the concordia and define a tight cluster (Fig. 4a).

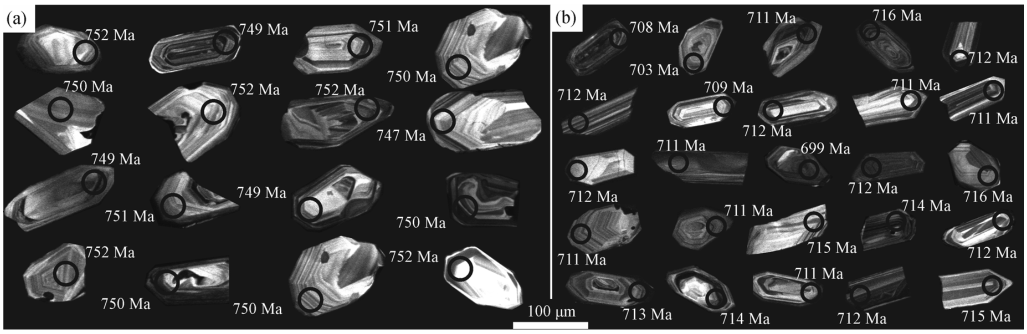

Fig. 3. Representative CL images of zircons from the diorite of the XJP (a), and the granite of the FQP (b).

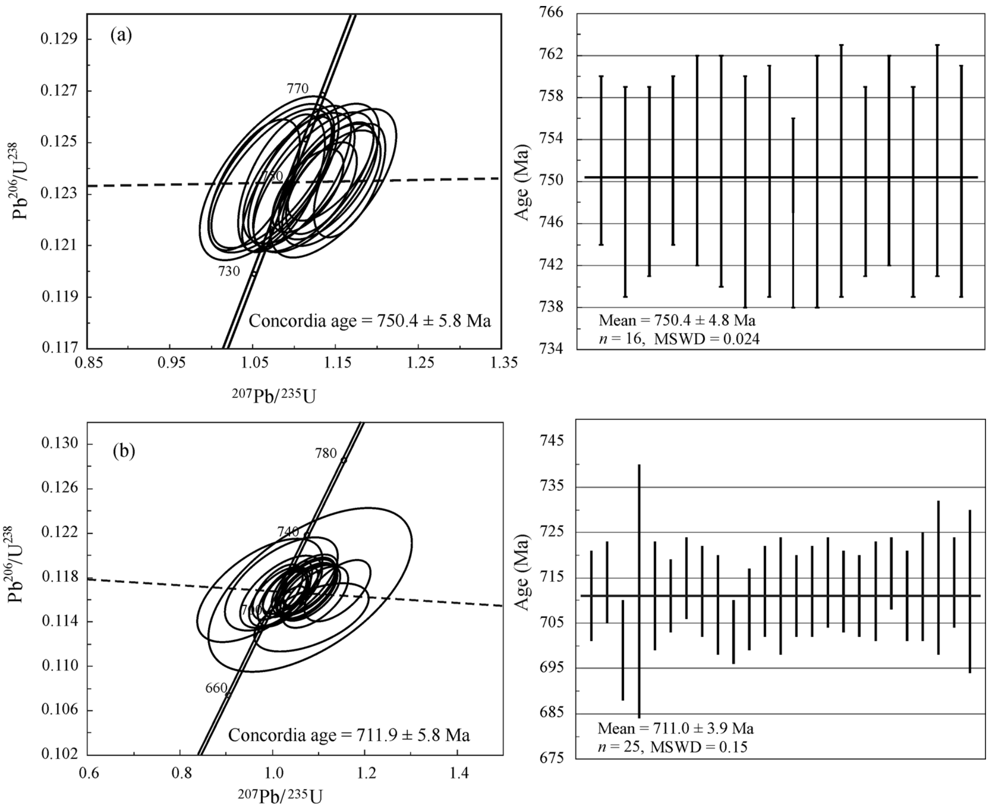

Fig. 4. Zircon U-Pb concordia age and the weighted mean $^{206}Pb/^{238}U$ age for the diorite of the XJP (a) and the granite of the FQP (b).

These data yield an average $^{206}Pb/^{238}U$ date of 750.4 ± 4.8 Ma (MSWD = 0.024). The remaining 14 points were rejected owing to discordant $^{207}Pb/^{235}U$ and $^{206}Pb/^{238}U$ data. The magmatic oscillatory zoning and high Th/U ratios of the zircons indicates that the achieved date represents the timing of formation of the diorite phase within the XJP. The majority of zircons from granite sample FQP-01 have concordant $^{207}Pb/^{235}U$ and $^{206}Pb/^{238}U$ ages (Fig. 4b), barring five analyses that were rejected as a result of $^{207}Pb/^{235}U$ and $^{206}Pb/^{238}U$ discordance. The remaining 25 concordant analyses yield a weighted mean $^{206}Pb/^{238}U$ age of 711 ± 3.9 Ma (MSWD = 0.15). Combining this age with the presence of magmatic zoning visible during CL imaging and the high Th/U ratios of these zircons indicates that the granite phase of the FPQ was emplaced at 711 ± 3.9 Ma.

4.2 Major and trace element geochemistry

4.2.1 Xiejiaba pluton

Samples from the XJP yield a nearly continuous range in compositions (Supp. Table 2). They contain 53.59–75.26 wt% SiO_2, 13.24–17.89 wt% Al_2O_3, 1.45–8.63 wt% TFe_2O_3, 0.18–4.01 wt% MgO, 2.53–6.07 wt% Na_2O, 1.10 –5.64 wt% K_2O, 0.50–7.00 wt% CaO, and 0.03–0.36 wt% P_2O_5. These samples have SiO_2 contents that negatively correlate with MgO, TFe_2O_3, Al_2O_3, CaO, P_2O_5, and TiO_2 (Fig. 5a–e). The samples are all classified as subalkaline in a total alkali vs. silica (TAS) diagram (Fig. 6a) and low-K to shoshonitic in a K_2O vs. SiO_2 diagram (Fig. 6b). They are metaluminous to peraluminous with A/CNK ratios (modal Al_2O_3/ (CaO + Na_2O + K_2O)) of 0.80–1.12 (Fig. 6c). They also have low $Mg^{\#}$ (100 × Mg/ (Mg + Fe)) values (14.46–48.28) that correlate negatively with SiO_2 concentrations.

Samples from the XJP contain total rare earth element (REE) contents of 65.9–167 ppm. They have low to moderately fractionated REE patterns with $(La/Yb)_N$ values of 2.99–13.3. All of these samples have similar chondrite-normalized REE patterns that are relatively enriched in light REEs (LREEs) relative to heavy REEs (HREEs) as well as negative or negligible Eu anomalies (Eu/Eu* = 0.69–1.05; Fig. 7a). Their primitive mantle-normalized multi-element variation diagram patterns show depletion in Nb, Ta, Ti, and P but enrichment in Ba, K, La, and Ce (Fig. 7b).

4.2.2 Fuqiangbei pluton

The FQP samples contain 69.42–76.76 wt% SiO_2, 13.05–14.88 wt% Al_2O_3, 1.17–2.85 wt% TFe_2O_3, 0.13–0.90 wt%, 3.89–6.45 wt% Na_2O, 0.76–3.44 wt% K_2O,

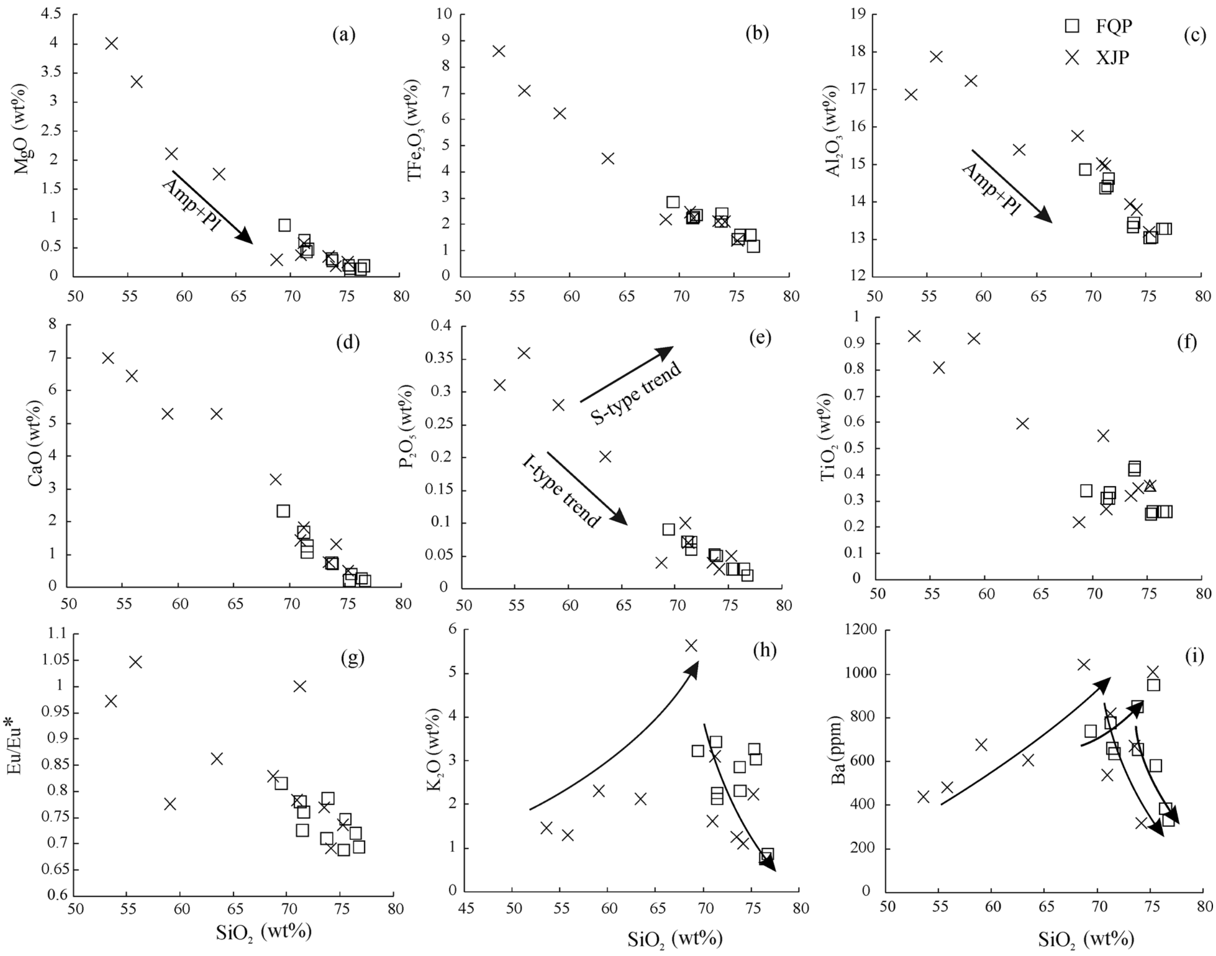

Fig. 5. Harker-type diagram showing variations in SiO_2 concentrations compared with selected major and trace element contents. Amp–amphibole; Pl–plagioclase.

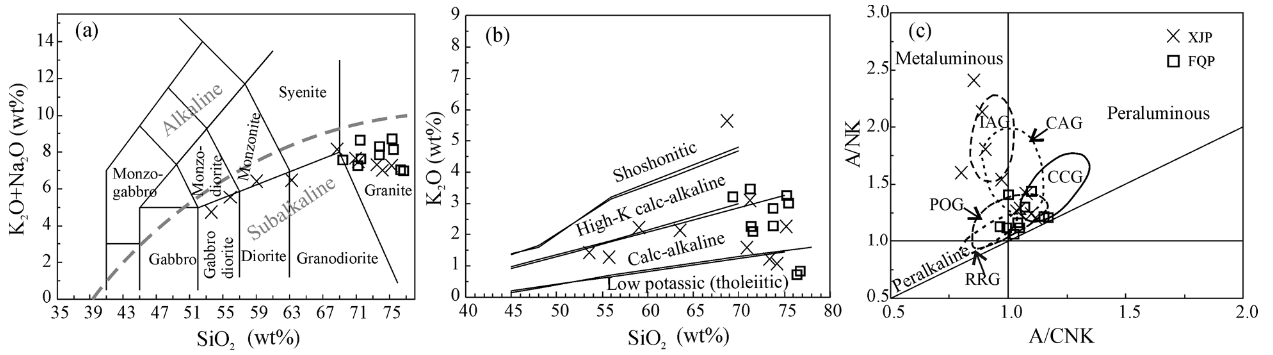

Fig. 6. SiO_2 vs. $Na_2O + K_2O$ (a), SiO_2 vs. K_2O (b), and A/NK vs. A/CNK (c) diagrams showing variations in the compositions of samples from the Niushan complex.
IAG–island-arc granotoid; CAG–continental arc granotoids; CCG–continental collisional granotoid; POG–post-orogenic granotoid; RRG–rift ridge grantoid.

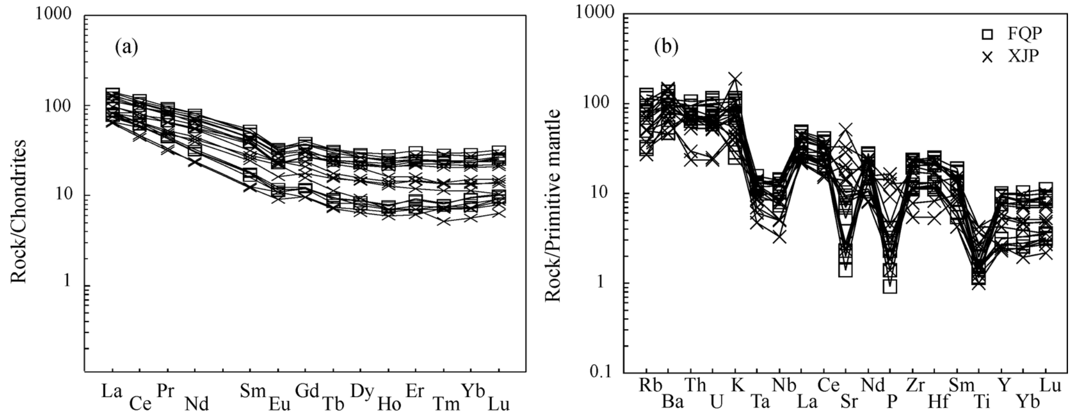

Fig. 7. Chondrite-normalized REE (a) and primitive mantle-normalized multi-element (b) variation diagrams for samples from the Niushan complex.
Chondrite-normalized values are from Boynton (1984). Primitive-mantle-normalized values are from Sun and McDonough (1989).

0.19–2.32 wt% CaO, and 0.02–0.09 wt% P_2O_5. Their SiO_2 concentrations negatively correlate with the MgO, TFe_2O_3, Al_2O_3, CaO, TiO_2, and P_2O_5 concentrations in these samples (Fig. 5a–f). All of these samples are classified as subalkaline in a TAS diagram (Fig. 6a) and low-K to high-K in a K_2O vs. SiO_2 diagram (Fig. 6b). They are metaluminous to peraluminous with A/CNK ratios of 0.99–1.17 (Fig. 6c) and have low $Mg^{\#}$ values (13.94–38.48) that correlate negatively with SiO_2 concentartions.

Samples from the FPQ have total REE contents of 84.4–189 ppm and low to moderately fractionated REE patterns with $(La/Yb)_N$ values of 3.56–10.9. All of these samples have similar chondrite-normalized REE patterns that are relatively enriched in LREEs relative to HREEs along with negative or negligible Eu anomalies (Eu/Eu* = 0.69–0.81; Fig. 7a). They also have primitive mantle-normalized multi-element variation diagram patterns that indicate depletion in Nb, Ta, Ti, and P and enrichment in Ba, K, La, and Ce (Fig. 7b).

4.3 Sr-Nd isotopic results

The results of the whole-rock Sr-Nd isotopic analysis are given in Table 1. The two FQP samples and the three XJP samples analyzed in this study have $^{87}Sr/^{86}Sr$ values of 0.704713–0.715067, $^{143}Nd/^{144}Nd$ ratios of 0.512245–0.512550, $^{87}Rb/^{86}Sr$ ratios of 0.153438–1.390235, and $^{147}Sm/^{144}Nd$ ratios of 0.103858–0.132905. Combining these data with the 750 Ma age of the XJP and the 711 Ma age for the FQP yields $(^{87}Sr/^{86}Sr)_i$ values of 0.700960–0.705693, $\varepsilon_{Nd}(t)$ values of 0.78–5.99, and two-stage Nd model ages of 1255–899 Ma.

Table 1 Sr-Nd isotopic analyses for the Niushan complex

Sample	Granite		Diorite		
	FQ-01	FQ-04	XJ-01	XJ-02	XJ-09
Rb (ppm)	79.7	72.4	41.9	31.9	66.9
Sr (ppm)	166	216	690	602	431
$^{87}Rb/^{86}Sr$	1.390235	0.970561	0.175834	0.153438	0.449455
$^{87}Sr/^{86}Sr$	0.715067	0.712437	0.705771	0.704713	0.710254
±2σ	0.000018	0.000019	0.000018	0.000018	0.000023
t (Ma)	711	711	750	750	750
$(^{87}Sr/^{86}Sr)_i$	0.700960	0.702588	0.703987	0.703156	0.705442
Sm (ppm)	2.44	2.78	6.69	4.28	1.86
Nd (ppm)	14.2	15.1	32.3	19.6	10.9
$^{147}Sm/^{144}Nd$	0.104582	0.112052	0.126060	0.132905	0.103858
$^{143}Nd/^{144}Nd$	0.512396	0.512550	0.512490	0.512541	0.512245
$(^{143}Nd/^{144}Nd)_i$	0.511909	0.512028	0.511870	0.511887	0.511734
$\varepsilon_{Nd}(t)$	3.661035	5.990033	3.895880	4.23482	1.241205
T_{DM2} (Ma)	1053	899	1147	1148	1255
$\varepsilon_{Sr}(t)$	−38.5429	−15.399	3.7421	−7.904	25.8007

5 Discussion

5.1 Petrogenesis and magma source

All of the samples from the Niushan complex have low loss-on-ignition (LOI) values (0.28–2.15) that indicate they have undergone only minor alteration, with both plagioclase and hornblende being visibly altered but to a limited extent. This indicates that the whole-rock geochemical and Sr-Nd isotopic data for these rocks can be used to constrain the petrogenesis and sourcing of the magmas that formed this complex.

5.1.1 Xiejiaba pluton

Although the XJP samples have a wide range of SiO_2 concentrations (53.59–75.26 wt%), the continuous major element trends shown in Harker-type diagrams for these samples (Fig. 5) and their similar chondrite-normalized REE and multi-element variation diagram patterns indicate that they are comagmatic. The diorite samples within this pluton have chondrite-normalized REE and primitive mantle-normalized multi element variation diagram patterns that show enrichment in LREEs and large ion lithophile elements (LILEs, e.g., K, Ba, and Sr) but depletion in Ti, Nb, Ta, and P, suggesting that they formed in a subduction-dominated environment (Pearce and Peate, 1995). Experimental research has determined that the melting of crustal metabasaltic rocks generates only low $Mg^{\#}$ (<40) melts (Rapp and Watson, 1995); the diorites in the study area, which have elevated MgO contents (1.76–4.01) and high $Mg^{\#}$ values (40.23–48.28) are inconsistent with that research. This means that these diorites cannot have been derived from a pure lower crustal source. Previous research also determined that subduction related intermediate to felsic magmas are usually derived from source regions containing a mixture of mantle wedge-derived and lower crustal magmas (Hildreth and Moorbath, 1988), which potentially represents the source of the diorites in the study area. Mantle-wedge material that overlies a subducted slab is almost always metasomatized by interaction with slab-derived fluids and other materials (Kepezhinskas et al., 1997; Zhao and Zhou, 2009). Such magmas derived from the resulting fluid-metasomatized mantle are generally enriched in LILEs and have high Ba contents, high Rb/Y, Sr/Nd, and Th/Zr ratios, and low Nb/Y, Th/Yb, and Nb/Zr ratios (Kepezhinskas et al., 1997), all of which characteristics are consistent with the diorite compositions from the XJP. This is exemplified by the fact that these diorites define fluid-related enrichment trends in Ba vs. Nb/Y, Rb/Y vs. Nb/Y, Th/Yb vs. Sr/Nd, and Nb/Zr vs. Th/Zr diagrams (Fig. 8), suggesting that they formed from magmas derived from a source that was metasomatized by interaction with slab-derived fluids. This indicates that the diorites in the study area formed from magmas derived

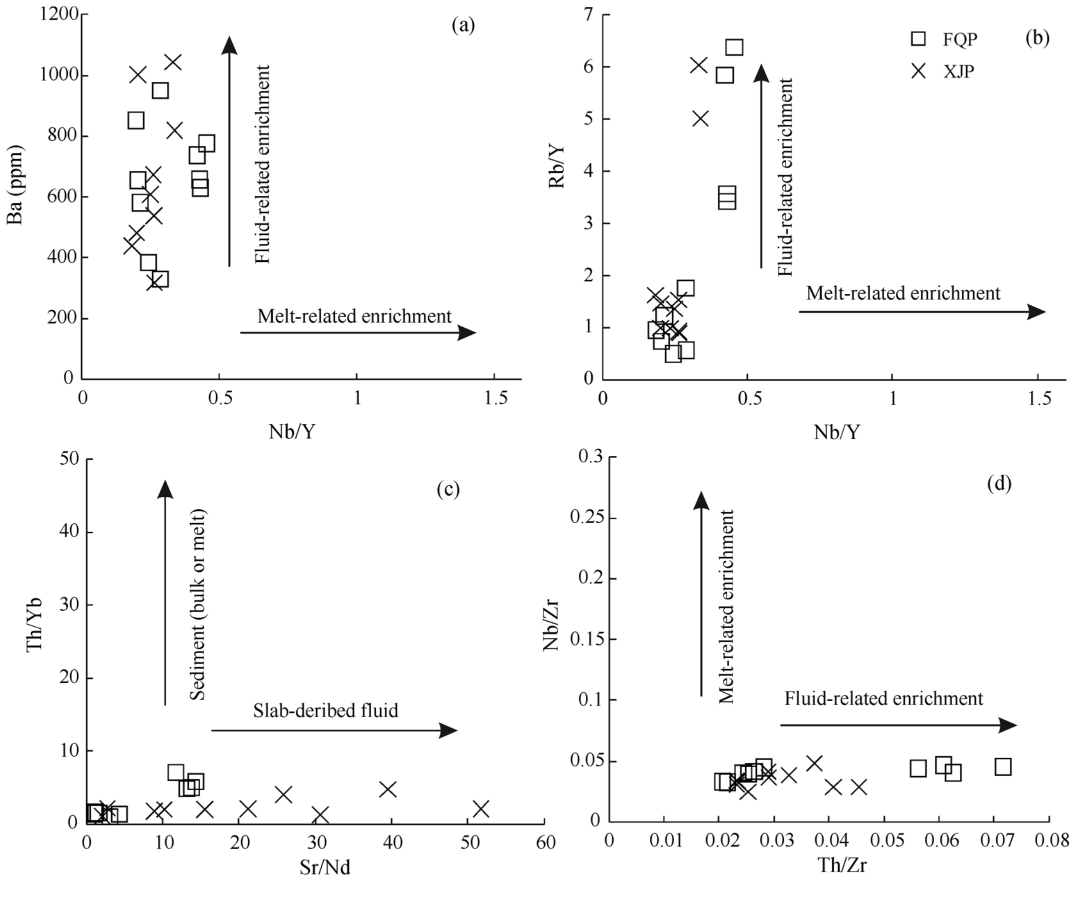

Fig. 8. Diagrams showing variations in (a) Ba vs. Nb/Y (after Kepezhinskas et al., 1997), (b) Rb/Y vs. Nb/Y (after Kepezhinskas et al., 1997), (c) Th/Yb vs. Sr/Nd (after Woodhead et al., 1998), and (d) Nb/Zr vs. Th/Zr (after Kepezhinskas et al., 1997) in samples from the study area.

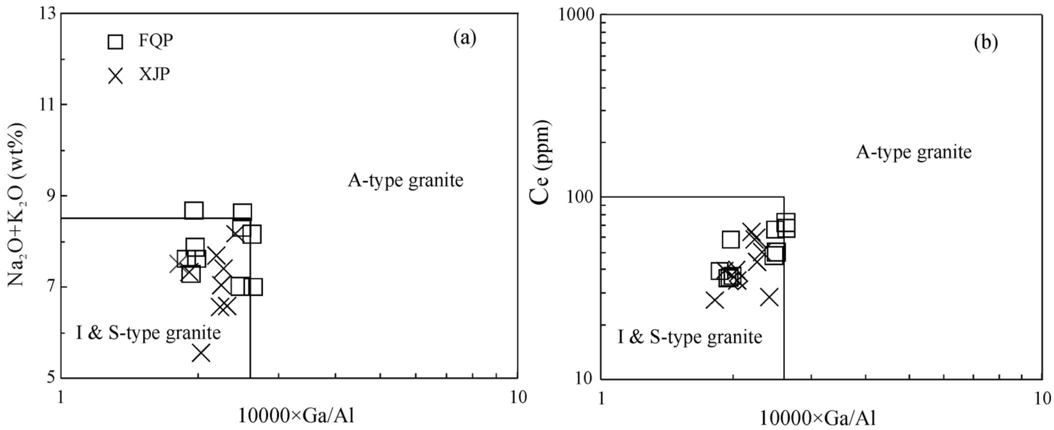

Fig. 9. Diagrams showing variations in (a) $Na_2O + K_2O$ vs. 10000 × Ga/Al and (b) Ce vs. 10000 × Ga/Al (Whalen et al., 1987) for samples from the study area.

from a source containing a mixture of hydrated mantle wedge and lower crustal material.

The granitoids within the XJP have similar chondrite-normalized REE and primitive-mantle normalized multi-element variation diagram patterns to those of the diorites in the study area, also suggesting that they were derived from the same source. Previous research indicated that granitoids can be divided into I-, S-, A-, and M-types (Whalen et al., 1987; Barbarin, 1999; Frost et al., 2001; Chappell and White, 2001). Samples from the Niushan complex are enriched in LREEs and LILEs, depleted in high field strength elements (HFSEs), have low A/CNK values (0.80–1.12), and contain hornblende, all of which indicate that they have an I-type affinity. The low 10000 × Ga/Al (Fig. 9) of these rocks precludes an A-type classification, and the negative correlation between P_2O_5 and SiO_2 contents (Fig. 5e) is also indicative of I-type rather than S-type affinity. The granitoids from the XJP are also classified as low-K to shoshonitic in a SiO_2 vs. K_2O diagram (Fig. 6b). I-type granitoids are generally formed by (1) mixing of mantle- and crust-derived magmas (Barbarin, 2005; Yang et al., 2007); (2) direct differentiation of mantle-derived basaltic magmas (Barth et al., 1995); or (3) partial melting of lower crustal metabasaltic rocks (Rapp et al., 1999). The continental crust is enriched in Na_2O, K_2O, Zr, Hf, Th, and LILEs and depleted in Nb, Ta, P_2O_5, and TiO_2 (Rapp and Watson, 1995), consistent with the geochemical composition of granitoids within the XJP. This indicates that the magmas that formed this intrusion cannot have been purely derived from a mantle source, but were instead derived from a mixed source containing mantle-derived magma. The samples also have low MgO, Cr, and Ni contents that are indicative of derivation from magmas generated by partial melting of lower continental crustal material. However, the geochemistry of these samples is also indicative of the involvement of slab-derived fluids (Fig. 8), indicating the involvement of a hydrated mantle-wedge source. Combining this with the geochemical similarities between the granitoids and diorites and the low $Mg^{\#}$ values (14.45–33.90) of the latter suggests that the granitoids formed from magmas derived from a mixed source containing hydrated mantle wedge and lower crustal material, with these magmas then undergoing significant differentiation prior to their emplacement within the complex as granitoids.

5.1.2 Fuqiangbei pluton

Granitoids from the FHP have similar chondrite-normalized REE and primitive mantle-normalized multi-element variation diagram patterns to the XJP samples, indicating that they formed from magmas derived from similar sources. The FHP granitoids also have relatively low A/CNK values (0.96–1.17) and $(La/Yb)_N$ ratios, relatively high LILE/HFSE ratios, and are depleted in Nb, Ta, Ti, and P, all of which are indicative of I-type granites formed in subduction-type environments. The FHP samples are enriched in Na_2O, K_2O, Zr, Hf, Th, and LILEs and depleted in Nb, Ta, P_2O_5, and TiO_2, and they have low $Mg^{\#}$ values (<40), all of which indicates derivation from melts generated by dehydration melting of lower crustal metabasaltic material (Rapp and Watson, 1995). This also rules out a model where these rocks formed from purely mantle-derived magmas, although it is likely that some contribution from these magmas was involved in the petrogenesis of the granitoids. The samples also have low MgO, Cr, and Ni contents, which indicate derivation from magmas generated by the partial melting of lower continental crust rather than mantle material. All of this suggests that the geochemical compositions of the samples from the Niushan pluton do not fit a genetic model involving the mixing of mantle- and crust-derived magmas or direct differentiation from mantle-derived basaltic magmas, but instead are consistent with the formation of the FQP from magmas originally generated by partial melting of lower continental crust. This is also consistent with the Sr-Nd isotopic compositions of the Niushan complex. Samples from this 750–711 Ma complex are similar to the contemporaneous Fenghuangshan (749–732 Ma) and Douling (750–709 Ma) plutons (Wang R R et al., 2019) in that all three intrusions have variable $\varepsilon_{Nd}(t)$ values and inconsistent initial $^{87}Sr/^{86}Sr$ ratios. These samples define trends that link the mantle array with YB lower crustal compositions (Fig. 10), suggesting that the magmas that formed these intrusions contained significant amounts of lower crustal material. The samples from the Niushan

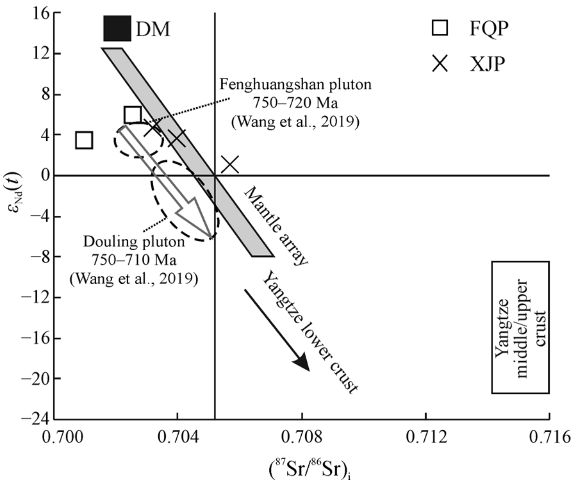

Fig. 10. Diagram showing variations in Sr-Nd isotopic compositions for samples from the Niushan pluton.

complex have positive ε_{Nd} (t = 750 and 711) values (1.24–5.99) and low ($^{87}Sr/^{86}Sr$)$_i$ values (0.700960–0.705442) that preclude the possibility of significant amounts of supracrustal mixing or the reworking of ancient crustal material, as the latter is often more isotopically enriched. Instead, the magmas that formed these intrusions were most likely derived from juvenile crustal sources or a source containing both juvenile crust and mantle material. The samples from the study area have average Ce/Pb (4.49) and Nb/Ta (14.90) ratios, which are close to the values expected for the crust but significantly different from those expected for mantle-derived magmas. Combining this with the Mg$^{\#}$ values of the diorites (40.23–48.28) and granitoids (14.46–33.90 for the XJP; 13.94–38.48 for the FQP) suggests that the magmas that formed the XJP were originally derived from a source containing juvenile crust mixed with mantle material, whereas the magmas that formed the FQP were derived from juvenile crust alone. This also supports the idea that the source of the magmas that formed the Niushan complex was generated during the formation of the Rodinia supercontinent, consistent with the 1255–899 Ma two-stage Nd model ages (T_{DM2}) of the samples from the study area.

The transition from intermediate to felsic rocks in the XJP is characterized by a general decrease in MgO, TFe_2O_3, Al_2O_3, CaO, P_2O_5, TiO_2, V, and Ni contents with a coincident increase in SiO_2 contents, all of which is indicative of significant fractional crystallization. The negative correlation between TFe_2O_3, Al_2O_3, P_2O_5, TiO_2, and Eu/Eu* with increasing SiO_2 contents (Fig. 5b–c, e–g) is indicative of the fractionation of plagioclase, Ti–Fe bearing minerals (ilmenite or rutile), and apatite. In addition, both K_2O and Ba initially increase before decreasing with increasing SiO_2 (Fig. 5h–i), suggesting that the magmas that formed the XJP initially fractionated plagioclase and amphibole before fractionating plagioclase, biotite, and K-feldspar. The rocks within the FQP are similar to those within the XJP with the exception of a decrease in K_2O concentrations with increasing SiO_2, suggesting that these magmas fractionated K-feldspar. This is consistent with variations in the Rb and Sr contents of these samples and their significantly negative Eu anomalies. The variable and relatively flat HREE patterns of these samples are also indicative of derivation from a source containing residual amphibole and garnet rather than just residual garnet. These geochemical characteristics indicate that the Niushan complex formed from magmas generated by the fractional crystallization of melts derived from the crust–mantle boundary.

All of the above suggests that the primitive magmas for the Niushan complex were derived from a source region containing a mixture of lower crustal material and mantle-derived melts, with the latter generated by the partial melting of juvenile lower crust. This melting was triggered by the addition of fluids released from subducted materials and the underplating of basaltic magma, triggering the melting of this hydrous source region. The melts then underwent fractional crystallization during their ascent and prior to their emplacement within the complex.

5.2 Tectonic setting

Previous research using zircon U-Pb geochronological data from the Neoproterozoic magmatic rocks in the study area showed that such rocks are found throughout the SQB (Zhang et al., 2004; Dong et al., 2017; Wang R R et al., 2019). Neoproterozoic magmatism in the SQB occurred during three periods (Zhang et al., 2004; Hu, 2013; Dong et al., 2017; Zhang et al., 2018; Wang R R et al., 2019), with peaks of ~860 (PI, 900–800 Ma), ~750 (PII, 800–670 Ma), and ~630 (PIII, 670–600 Ma), all of which relate to the evolution of Rodinia and subduction along continental margins. The magmatism prior to PIII is thought to have been linked with lithospheric extension associated with the breakup of Rodinia (Zhu et al., 2014a, b) or a back-arc rift setting (Guo et al., 2014; Wang et al., 2016). However, the middle Neoproterozoic tectonic background and Neoproterozoic evolution of the northern margin of the YB and SQB remain controversial, with intracontinental rift, rift-related plume, and subduction type models all suggested to date (Zhao and Cawood, 2012). The plume-related rifting and intracontinental rift models suggest that the tectonism was related to the breakup of the Rodinia supercontinent (Li H K et al., 2003; Li Z X et al., 2003; Wang and Li, 2003; Wang et al., 2011a, b). In comparison, the subduction model reflects the presence of Neoproterozoic arc-related igneous rocks within the western and northern margins of the YB (Zhou et al., 2002a, b; Wang et al., 2004, 2007; Zhao et al., 2010).

Recent research on the contemporaneous rocks in the study area has identified numerous arc- or subduction-related extrusive and intrusive rocks in areas such as the Xiaomoling and Douling complexes (783–730 Ma; Ling et al., 2008; Xia et al., 2008; Zhu et al., 2008) of the northern South Qinling region, the Wudang Group rhyolites within the Wudangshan, Douling, and Fenghuangshan areas (783–730 Ma; Ling et al., 2008; Xia et al., 2008; Zhu et al., 2008), intrusions within the southern South Qinling area (797–743 Ma; Li et al., 2012), rhyodacitic tuff and metatrachyandesite of the Suixian Group in the Tongbaishan area (763–741 Ma), and the Hannan complex in the northwestern YB (825–706 Ma; Dong et al., 2012). Yang et al. (2012) suggested that the SQB records

Neoproterozoic subduction, as evidenced by a comparison of geochronological data for the Tiewadian pluton (742–704 Ma) and the Hannan complex. Although this research suggests that the Neoproterozoic magmatic rocks within the margins of the YB, including the SQB, formed as a result of long-lived subduction or within an active continental margin setting, i.e., an accretionary orogen, the tectonic evolution of this area, especially the timing transition between compression and extension and the related tectonic processes, requires further research. In addition, possible evidence supporting a mantle plume model, include radiating dike swarms, voluminous basalts, and crustal doming, is absent from this region (Zhou et al., 2002a; Zhao et al., 2011).

The Niushan complex was originally thought to formed during the Triassic (Team No. 1, Shaanxi Bureau of Geology and Mineral Resources, 2017). Our new zircon U-Pb dating indicates that the complex actually formed at 750–711 Ma, during the PII phase of magmatism (Zhang et al., 2018) in the SQB, meaning that this complex can provide new insights into the late Neoproterozoic tectonic evolution from compression (PII) to extension (PIII) and the related tectonic mechanism of the South Qinling area. The granitoids of the Niushan complex have calc-alkaline I-type granite affinities, are enriched in both LREEs and LILEs, have relatively low A/CNK values, and are depleted in Nb, Ta, P, and Ti. All of these characteristics are indicative of a subduction- or arc-type affinity (Pearce and Peate, 1995). Their relatively low Sr/Y (0.86–38.90; Fig. 11a) and $(La/Yb)_N$ (2.99–13.30; Fig. 11b) ratios and variable Y and Yb_N values are inconsistent with adakite and tonalite-trondhjemite-granodiorite (TTG)-type affinities but instead indicate that the Niushan samples have compositions similar to magmas generated in modern arc settings (Defant and Drummond, 1990; Petford and Atherton, 1996). This is consistent with their low MgO (0.13–4.01 wt%), Cr (5.28–32.8 ppm barring a single sample containing 62.8 ppm), and Ni (1.24–29.7 ppm) contents and $Mg^{\#}$ values (13.9–48.3). Samples from the Niushan pluton plot in the arc magmatic field of tectonic discrimination diagrams (Fig. 12a, b), and the 750 Ma XJP and 711 Ma FQP samples plot in the pre-plate collision and syn-collision and post-orogenic fields of an R1 vs. R2 diagram, respectively (Fig. 12c). This probably records the tectonic evolution of the study area from subduction to late subduction settings between 750 and 711 Ma. All of this suggests that the Neoproterozoic intrusions in this region have arc-type geochemical affinities, although it remains controversial whether this magmatism occurred in an island or continental arc setting (Yan et al., 2010; Bader et al., 2013; Ao et al., 2014; Zhu et al., 2014b; Dong et al., 2017; Li et al., 2018; Zhao et al., 2018).

Recent research has provided increasing evidence that the northern margin of the YB and the South Qinling area record continental arc-type tectonism and magmatism, as follows: (1) the presence of 790–780 Ma Neoproterozoic volcanic and sedimentary rocks that crop out along the Chengkou–Fengxi fault, which forms the boundary between northern margin of the YB and the South Qinling area. These rocks formed in a continental arc setting but were deposited in an associated forearc basin (Yan et al., 2010); (2) the Hannan complex in the northern margin of the YB formed as a result of multiple stages of Neoproterozoic subduction within an active continental margin setting (Gao et al., 1990; Zhou et al., 2002a, b; Ling et al., 2003; Zhao and Zhou, 2008; Zhao et al., 2008, 2018; Dong et al., 2012; Bader et al., 2013; Ao et al., 2014; Li et al., 2018), with a 790 Ma gabbro in this complex recording the assimilation of continental crustal material by mantle-derived magma (Xiang et al., 2015); (3) the contemporaneous Douling (750–709 Ma) and Fenghuangshan (749–728 Ma) plutons in the study area are known to have formed in a continental arc-type tectonic setting (Wang et al., 2019); (4) the Suixian Group (700–680 Ma) in the South Qinling area also formed in a continental-arc setting and contains continent-derived material (Liu et al., 2018); and (5) volcanic-sedimentary rocks and plutonic complexes with well-defined arc signatures have been identified along other margins of the YB, especially the northern margin. In summary, the 820–780 Ma Wangjiangshan and Bijikou complexes in the Hannan area have arc-type affinities that are indicative of formation in an active arc setting along a continental margin (Zhou et al., 2002a, 2007; Dong et al., 2011a, b). The new data from the Niushan complex are consistent with this tectonic setting, as exemplified by the low A/

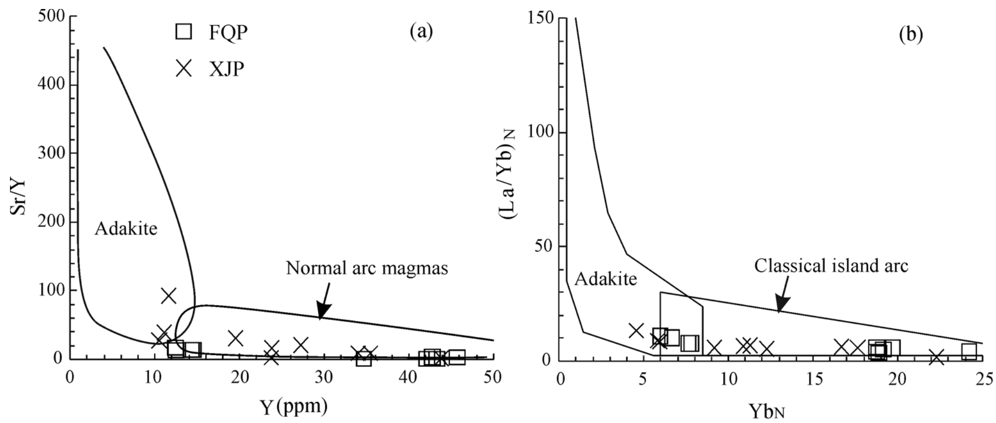

Fig. 11. Diagrams showing variations in the (a) Sr/Y vs. Y (Defant and Drummond, 1990) and (b) $(La/Yb)_N$ vs. Yb_N (Martin, 1999) compositions of samples from the Niushan complex.

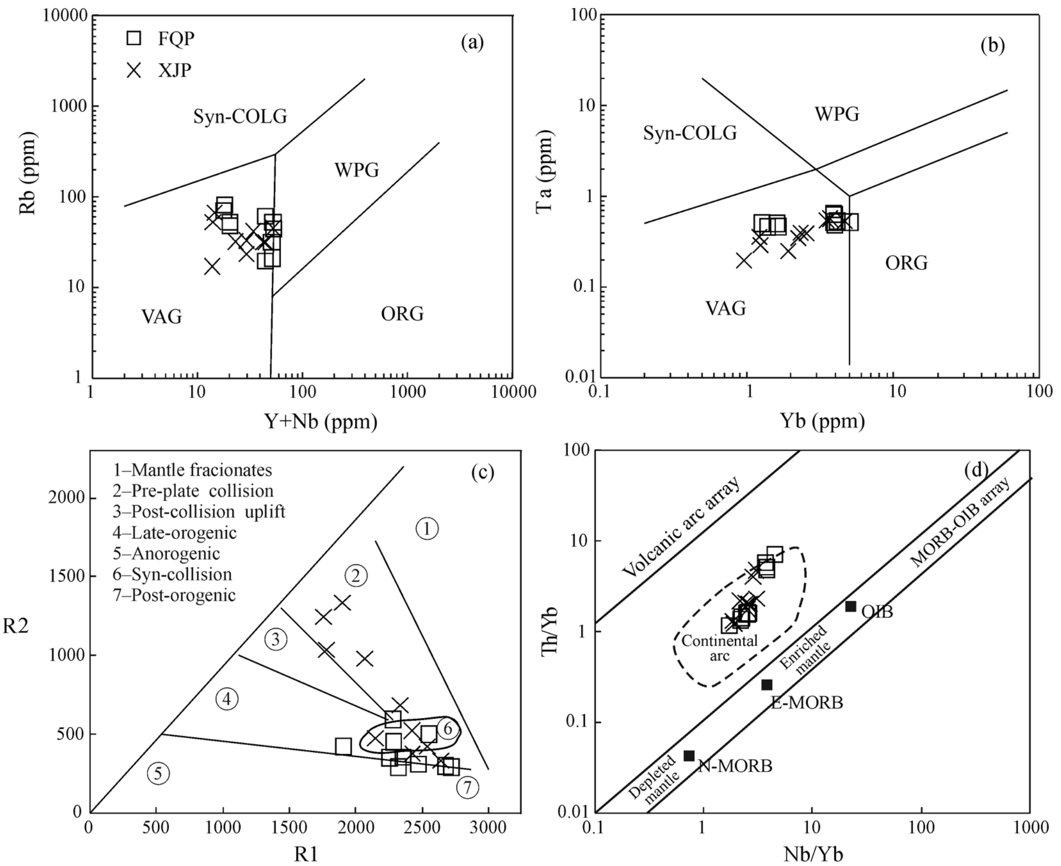

Fig. 12. Tectonic discrimination diagrams showing possible tectonic settings for the magmatism that formed the Niushan complex: (a) Rb vs. Y + Nb (after Pearce et al., 1984); (b) Ta vs. Yb (after Pearce et al., 1984); (c) R1-R2; (d) Th/Yb vs. Nb/Yb.

CNK (0.80–1.17) and moderate A/NK (1.05–2.41) values of the rocks. This indicates that they have continental arc granitoid (CAG) rather than typical island-arc granitoid (IAG) affinities (Fig. 6c), with all of these samples plotting in the continental-arc field of a tectonic discrimination diagram (Fig. 12d). All of this supports the presence of a late Neoproterozoic (750–711 Ma) continental-arc setting within the northern margin of the YB and South Qinling area.

5.3 Other comparative evidence

Although this study provides evidence of long-lived Neoproterozoic subduction (900–700 Ma; Dong and Santosh, 2016) at the northern margin of the YB and the South Qinling area, the later stages of subduction in this region have not yet been reconstructed. Igneous rocks in the study area and adjacent regions may provide opportunities to better constrain the later stages of the tectonic history. For example, evidence of Neoproterozoic subduction to the north of the study area along the Bikou–Xiaomoling–Douling suture is provided by the Banbanshan granite (730 Ma; Wu et al., 2012). To the south, Neoproterozoic granitic and dioritic intrusions within the Fenghuangshan area yield ages of 797–743 Ma and have arc-type geochemical affinities (Li et al., 2012). The Wudang Group within the Douling, Wudangshan and Fenghuangshan areas yield ages of 780–730 (Zhu et al., 2008), 783 ± 4.9 (Xia et al., 2008), and 769–752 Ma (Ling et al., 2008), constraining the timing of subduction to 783–730 Ma (Dong and Santosh, 2016). The arc-related intrusions of the Hannan complex in the northern margin of the YB also yield ages of 819–746 Ma (Zhou et al., 2002a; Zhao and Zhou, 2009; Zhao et al., 2010). This Neoproterozoic subduction event is further supported by the geochemical characteristics of 763 ± 7 and 741 ± 7 Ma volcanic rocks in the Suixian Group in the eastern South Qinling area (Xue et al., 2011). All of these data indicate that the subduction recorded in the SQB and northern margin of the YB ceased at around 750–730 Ma.

Previous studies on the magmatic rocks in the SQB, NCC, and SCC have generally reported negative $\varepsilon_{Hf}(t)$ values for rocks formed between ca. 850 and 750 Ma and positive $\varepsilon_{Hf}(t)$ values for rocks formed after 750 Ma (Wang R R et al., 2019). This provides evidence of the significant involvement of ancient crustal material during subduction and the later initiation of regional-scale extension within a back-arc setting (Wang R R et al., 2019), although subduction still persisted at this time. Our new age data indicate that the Niushan pluton formed at 750–711 Ma. As shown, samples from this complex have relatively low Al_2O_3/(FeO + MgO + TiO_2) and CaO/(FeO + MgO + TiO_2) ratios that, when considered alongside their flat HREE patterns (Fig. 7a) and significant Eu and Sr depletions (Fig. 7a, b), are indicative of low-pressure melting (Fig. 13). This means that the magmas that formed the Niushan pluton formed under low-pressure conditions,

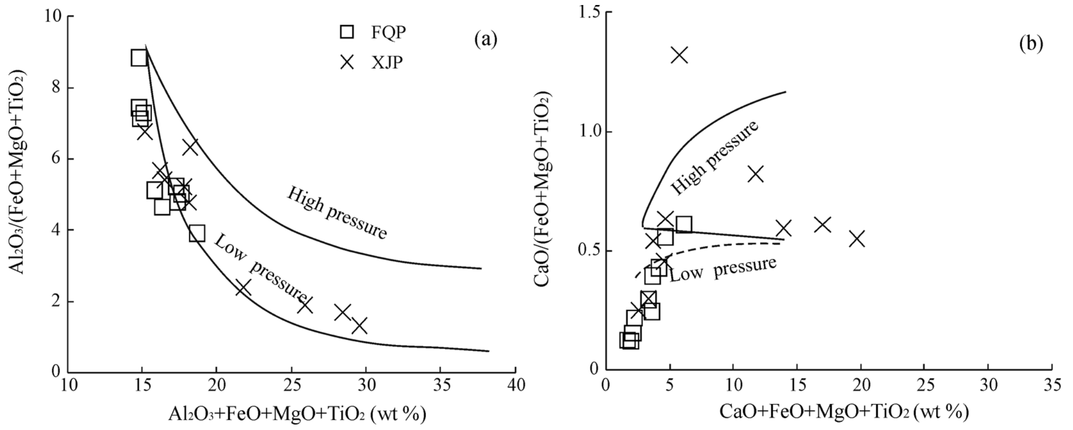

Fig. 13. Diagrams showing variations in the composition of samples from the Niushan complex (after Patiňo Douce, 1999).

indicating the necessary involvement of fluids or melts during the formation of these magmas (Miller et al., 2003). This is consistent with the high Th/Zr and Rb/Y and low Nb/Zr and Nb/Y ratios of the samples from the complex (Fig. 8a–d). The contemporaneous Fenghuangshan pluton is thought to have formed from magmas initially generated at low temperatures and pressures with a transition to formation from magmas generated under higher temperature but similar low-pressure conditions (Wang R R et al., 2019). This evolution of melting conditions within a subduction environment reflects the dehydration of subducted slab material and subsequent back-arc extension and associated upwelling of asthenospheric mantle material. Metasomatism by fluids derived from a subducted slab and the later underplating of the region by basaltic magmas can cause low pressure melting during the evolution from both arc to back-arc conditions (Ducea et al., 2015). This means that the SQB and the northern margin of the YB record the predominant tectonic transit from an arc to a back-arc tectonic setting at 750–711 Ma (Fig. 14). Combining this with the fact that the 750 Ma magmatic rocks in this region are generally bimodal (Ling et al., 2002a; Zheng et al., 2006; Zhu et al., 2014a), with some having arc-type alkaline affinities (Lu et al., 1999; Ling et al., 2002b; Chen et al., 2006; Zhu et al., 2014b) and others being parts of mafic dike swarms (Ling et al., 2008), suggests that Neoproterozoic continental rifting occurred along the northern margin of the YB and the SQB (Zheng et al., 2004; Fu et al., 2012; Liu and Zhang, 2013; Zhang and Zheng, 2013). In comparison, ca. 765 Ma mafic magmatic rocks in the Guibei and Xiangxi areas record a single continental rift setting (Zhou et al., 2007) within the southern YB.

Integrating the new data presented in this study with the results of previous research suggests that Neoproterozoic backarc extension overprinted existing continental rift-type tectonism within the northern margin of the YB and the SQB. The single continental rift within the southern YB also suggests that this block was located at the margin of the Rodinia supercontinent with a northern margin that faced the exterior ocean (Yang et al., 2004; Evans, 2009; Cawood et al., 2013). This setting continued until the Ediacaran, when the final breakup of Rodinia caused the

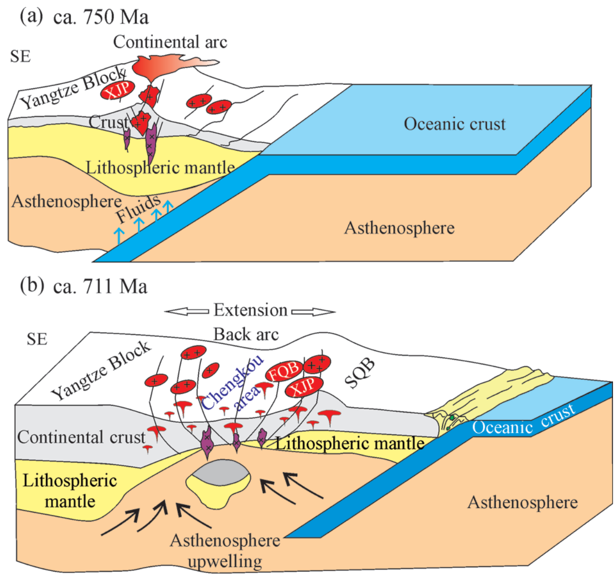

Fig. 14. Diagramatic models of the tectonic evolutionary history of the northern margin of the Yangtze Block during the Neoproterozoic (750–711 Ma).

separation of the SQB from the YB, as recorded in the Chengkou area (Wang et al., 2020).

6 Conclusions

The new petrological, geochronological, and geochemical data for the Niushan complex presented in this study allow us to conclude the following:

(1) The XJP and FQP samples from the Niushan complex yield zircon U-Pb ages of 750 and 711 Ma, respectively. The Sr-Nd isotopic and whole-rock geochemical compositions of these samples are indicative of formation from low-pressure melts derived from the crust–mantle boundary;

(2) 750–711 Ma arc-related intermediate to felsic rocks from the XJP and FQP within the Niushan complex provide evidence of an active continental margin system along the SQB, which evolved from an arc to a back-arc setting between 750 and 711 Ma;

(3) Combining the new data presented in this study with the results of previous research on Neoproterozoic rocks within the South Qinling belt and the northern margin of the Yangtze Block suggest that this region records both subduction and intracontinental rifting, with the SQB located within the margin of the Rodinia supercontinent, with a northern margin that faced the exterior ocean.

Acknowledgments

This work was supported by the National Natural Science Foundation of China (Grant No. 41872219), the Key Research and Development Program of Shaanxi (Grant No. 2019SF-245), the Natural Science Foundation of Shaanxi Province (Grant No. 2023-JC-YB-222), and an integrated research project of Integrated Exploration of China Geological Survey (Grant No. WKZB1911BJM300369/002). We are grateful to Dr. Yu Xiaofei from the Development and Research Center of China Geological Survey for providing constructive suggestions, which have been very helpful to this manuscript.

Manuscript received Aug. 26, 2021
accepted Mar. 13, 2022
associate EIC: XIAO Wenjiao
edited by Susan TURNER and GUO Xianqing

Supplementary data to this article can be found online at http: //doi.org/10.1111/1755-6724.14926.

References

Andersen, T., 2002. Correction of common lead in U-Pb analyses that do not report ^{204}Pb. Chemical Geology, 192: 59–79.

Ao, W.H., Zhang, Y.K., Zhang, R.Y., Zhao, Y., and Sun, Y., 2014. Neoproterozoic crustal accretion of the northern margin of Yangtze plate: Constrains from geochemical characteristics, LA-ICP-MS zircon U-Pb chronology and Hf isotopic compositions of trondhjemite from Zushidian area, Hannan region. Geological Review, 60(6): 1393–1408 (in Chinese with English abstract).

Ao, W.H., Zhao, Y., Zhang, Y.K., Zhai, M.G., Zhang, H., Zhang, R.Y., Wang, Q., and Sun, Y., 2019. The Neoproterozoic magmatism in the northern margin of the Yangtze Block: Insights from Neoproterozoic (950–706 Ma) gabbroic-granitoid rocks of the Hannan Complex. Gondwana Research, 333: 105442.

Bader, T., Ratschbacher, L., Franz, L., Yang, Z., Hofmann, M., Linnemann, Ulf, and Yuan, H.L., 2013. The heart of China revisited, I. Proterozoic tectonics of the Qin mountains in the core of supercontinent Rodinia. Tectonics, 32(3): 661–687.

Barbarin, B., 1999. A review of the relationships between granitoid types, their origins and their geodynamic environments. Lithos, 46: 605–626.

Barbarin, B., 2005. Mafific magmatic enclaves and mafific rocks associated with some granitoids of the central Sierra Nevada batholith, California: Nature, origin, and relations with the hosts. Lithos, 80: 155–177.

Barth, A.P., Wooden, J.L., Tosdal, R.M., and Morrison, J., 1995. Crustal contamination in the petrogenesis of a calc-alkalic rock series: Josephine Mountain intrusion, California. Geological Society of America Bulletin, 107: 201–212.

Boynton, W.V., 1984. Cosmochemistry of the rare earth elements: Meteorite studies. In: Henderson, P. (ed.), Rare Earth Element Geochemistry. Elservier, 63–114.

Cawood, P.A., Wang, Y.J., Xu, Y.J., and Zhao, G.C., 2013. Locating south China in Rodinia and Gondwana: A fragment of greater India lithosphere? Geology, 41(8): 903–906.

Chappell, B.W., and White, A.J.R., 2001. Two contrasting granite types: 25 years later. Australian Journal of Earth Sciences, 48: 489–499.

Chen, Z.H., Lu, S.N., Li, H.K., Li, H.M., Xiang, Z.Q., Zhou, H.Y., and Song, B., 2006. Constraining the role of the Qinling orogen in the assembly and break-up of Rodinia: Tectonic implications for Neoproterozoic granite occurrences. Journal of Asian Earth Sciences, 28: 99–115.

Defant, M.J., and Drummond, M.S., 1990. Derivation of some modern arc magmas by melting of young subducted lithosphere. Nature, 347: 662–665.

Dong, Y.P., and Santosh, M., 2016. Tectonic architecture and multiple orogeny of the Qinling orogenic belt, central China. Gondwana Research, 29: 1–40.

Dong, Y.P., Liu, X.M., Santosh, M., Chen, Q., Zhang, X.M., Li, W., He, D.F., and Zhang, G.W., 2012. Neoproterozoic accretionary tectonics along the northwestern margin of the Yangtze Block, China: Constraints from zircon U-Pb geochronology and geochemistry. Precambrian Research, 196–197: 247–274.

Dong, Y.P., Liu, X.M., Neubauer, F., Zhang, G.W., Tao, N., Zhang, Y.G., Zhang, X.N., and Li, W., 2013. Timing of Paleozoic amalgamation between the North China and South China Blocks: Evidence from detrital zircon U-Pb ages. Tectonophysics, 586: 173–191.

Dong, Y.P., Yang, Z., Liu, X.M., Zhang, X.N., He, D.F., Li, W., Zhang, F.F., Sun, S.S., Zhang, H.F., and Zhang, G.W., 2014. Neoproterozoic amalgamation of the Northern Qinling terrain to the North China Craton: Constraints from geochronology and geochemistry of the Kuanping ophiolite. Precambrian Research, 255: 77–95.

Dong, Y.P., Zhang, G.W., Lai, S.C., Zhou, D.W., and Zhu, B.Q., 1999. An ophiolitic tectonic melange fifirst discovered in Huashan area, south margin of Qinling orogenic belt, and its tectonic implications. Science in China (Series D), 42: 292–302.

Dong, Y.P., Liu, X.M., Santosh, M., Zhang, X.N., Chen, Q., Yang, C., and Yang, Z., 2011a. Neoproterozoic subduction tectonics of the northwestern Yangtze Block in South China: Constrains from zircon U-Pb geochronology and geochemistry of mafic intrusions in the Hannan Massif. Precambrian Research, 189: 66–90.

Dong, Y.P., Zhang, G.W., Neubauer, F., Liu, X.M., Genser, J., and Hauzenberger, C., 2011b. Tectonic evolution of the Qinling orogen, China: Review and synthesis. Journal of Asian Earth Sciences, 41: 213–237.

Dong, Y.P., Zhang, G.W., Neubauer, F., Liu, X.M., Genser, J., and Hauzenberger, C., 2011c. Tectonic evolution of the Qinling orogen, China: Review and synthesis. Journal of Asian Earth Sciences, 41: 213–237.

Dong, Y.P., Sun, S.S., Yang, Z., Liu, X.M., Zhang, F.F., Li, W., Cheng, B., He D.F., and Zhang, G.W., 2017. Neoproterozoic subduction-accretionary tectonics of the South Qinling Belt, China. Precambrian Research, 293: 73–90.

Ducea, M.N., Saleeby, J.B., and Bergantz, G., 2015. The architecture, chemistry, and evolution of continental magmatic arcs. Annual Review of Earth and Planetary Sciences, 43: 299–331.

Evans, D.A.D., 2009. The palaeomagnetically viable, long-lived and all-inclusive Rodinia supercontinent reconstruction. Geological Society, London, Special Publications, 327: 371–404.

Frost, B.R., Barnes, C.G., Collins, W.J., Arculus, R.J., Ellis, D.J., and Frost, C.D., 2001. A geochemical classification for granitic rocks. Journal of Petrology, 42: 2033–2048.

Fu, B., Kita, N.T., Wilde, S.A., Liu, X., Cliffff, J., and Greig, A., 2012. Origin of the Tongbai–Dabie–Sulu Neoproterozoic low-δ^{18}O igneous province, east-central China. Contributions to Mineralogy and Petrology, 165: 641–662.

Gao, S., Zhang, B.R., and Li, Z.J., 1990. Geochemical evidence for Proterozoic continental arc and continental margin rift magmatism along the northern margin of the Yangtze Craton, South China. Precambrian Research, 47: 205–221.

Guo, X.Q., Yan, Z., Wang, Z.Q., Fu, C.L., and Chen, L., 2014. Tectonic setting of Lijiabian Ti-Fe deposit in Shanyang-

Zhashui ore concentration area, Qinling Orogen. Acta Petrologica Sinica, 30(2): 437–450 (in Chinese with English abstract).

Hildreth, W., and Moorbath, S., 1988. Crustal contribution to arc magmatism in the Andes of Central Chile. Contributions to Mineralogy and Petrology, 98: 455–489.

Hu, J., 2013. Study on metamorphism and geochronology of the Douling Complex, South Qinling Orogen (Ph.D. thesis). Chinese Academy of Geological Sciences, 1–123 (in Chinese with English abstract).

Kepezhinskas, P., Mcdermott, F., Defant, M.J., Hochstaedter, A., Drummond, M.S., Hawkesworth, C.J., Koloskov, A., Maury, R.C., and Bellon, H., 1997. Trace element and Sr-Nd-Pb isotopic constraints on a three-component model of Kamchatka arc petrogenesis. Geochimica et Cosmochimica Acta, 61: 577–600.

Kinny, P.D., Wijbrans, J.R., Froude, D.O., Williams, I.S., and Compston, W., 1990. Age constraints on the geological evolution of the Narryer Gneiss Complex, Western Australia. Australian Journal of Earth Sciences, 37: 51–69.

Li, J.H., Zhang, Y.Q., Xu, X.B., Dong, S.W., and Li, T.D., 2012. Zircon U-Pb LA-ICP-MS dating of Fenghuangshan pluton in Northern Daba Mountains and its implications to tectonic settings. Geological Review, 58(2): 581–593 (in Chinese with English abstract).

Li, Z.X., Zhang, L., and Powell, C.M., 1995. South China in Rodinia: Part of the missing link between Australia-East Antarctica and Laurentia? Geology, 23: 407–410.

Li, S.G., Sun, W.D., and Zhang, G.W., 1996. Chronology and geochemistry of metavolcanic rocks from Heigouxia valley in Mian–Lüe tectonic belt, South Qinling: Evidence for a Paleozoic oceanic basin and its close time. Science in China (Series D), 39: 300–310.

Li, Z.X., Li, X.H., Kinny, P.D., and Wang, J., 1999. The breakup of Rodinia: Did it start with a mantle plume beneath South China? Earth and Planetary Science Letters, 173: 171–181.

Li, H.K., Lu, S.N., Chen, Z.H., Xiang, Z.Q., Zhou, H.Y., and Hao, G.J., 2003. Zircon U-Pb geochronology of rift-type volcanic rocks of the Yaolinghe Group in the South Qinling orogen. Geological Bulletin of China, 22: 775–781 (in Chinese with English abstract).

Li, Z.X., Li, X.H., Kinny, P.D., Wang, J., Zhang, S., and Zhou, H., 2003. Geochronology of Neoproterozoic syn-rift magmatism in the Yangtze Craton, South China and correlations with other continents: Evidence for a mantle superplume that broke up Rodinia. Precambrian Research, 122: 85–109.

Li, J.Y., Wang, X.L., and Gu, Z.D., 2018. Early Neoproterozoic arc magmatism of the Tongmuliang Group on the northwestern margin of the Yangtze Block: Implications for Rodinia assembly. Precambrian Research, 308: 181–197.

Ling, W.L., Gao, S., Ouyang, J.P., Zhang, B.R., and Li, H.M., 2002a. Time and tectonic setting of the Xixiang Group: Constraints from zircon U-Pb geochronology and geochemistry. Science in China (Series D), 45: 818–831.

Ling, W.L., Cheng, J.P., and Wang, X.H., 2002b. Geochemical features of the Neoproterozoic igneous rocks from the Wudang region and their implications for the reconstruction of the Jinning tectonic evolution along the South Qinling orogenic belt. Acta Petrologica Sinica, 18: 25–36 (in Chinese with English abstract).

Ling, W.L., Gao, S., Zhang, B.R., Li, H.M., Liu, Y., and Cheng, J.P., 2003. Neoproterozoic tectonic evolution of the northwestern Yangtze craton, South China: Implications for amalgamation and break-up of the Rodinia Supercontinent. Precambrian Research, 122: 111–140.

Ling, W.L., Ren, B.F., Duan, R.C., Liu, X.M., Mao, X.W., Peng, L.H., Liu, Z.X., Cheng, J.P., and Yang, H.M., 2008. Timing of the Wudangshan, Yaolinghe volcanic sequences and mafific sills in South Qinling: U-Pb zircon geochronology and tectonic implication. Chinese Science Bulletin, 53: 2192–2199.

Liu, H., Shao, J.H., Cawood, P.A., and Wang, W., 2018. South China in Rodinia: Constrains from the Neoproterozoic Suixian volcano-sedimentary group of the South Qinling belt. Precambrian Research, 314: 170–193.

Liu, J., and Zhang, L., 2013. Neoproterozoic low to negative $\delta^{18}O$ volcanic and intrusive rocks in the Qinling Mountains and their geological signifificance. Precambrian Research, 230: 138–167.

Lu, X.X., Wei, X.D., Xiao, Q.H., Zhang, Z.Q., Li, H.M., and Wang, W., 1999. Geochronological studies of rapakivi granites in the Qinling and its geological implications. Journal of China University of Geosciences, 15(4): 372–377 (in Chinese with English abstract).

Ludwig, K., 2003. Isoplot/Ex, Version 3: A Geochronological toolkit for microsoft excel: Berkeley. California, Geochronology Center Berkeley.

Martin, H., 1999. Adakitic magmas: Modern analogues of Archean granitoids. Lithos, 46(3): 411–429.

Miller, C.F., McDowell, S.M., and Mapes, R.W., 2003. Hot and cold granites? Implications of zircon saturation temperatures and preservation of inheritance. Geology, 6: 529–532.

Nie, H., Ye, R.S., Cheng, H., Zhu, X.Y., and Chen, F.K., 2019. Neoproterozoic intrusions along the northern margin of South Qinling, central China: Geochemistry, zircon ages, and tectonic implications. Precambrian Research, 334: 105406.

Patiño Douce, A.E., 1999. What do experiments tell us about the relative contributions of crust and mantle to the origin of granitic magmas? In: Castro, A., Fernandez, C., and Vigneresse, J.L. (eds.), Understanding Granites: Integrating New and Classical Techniques. Geological Society, London. Special Publications, 168(1): 55–75.

Pearce, J.A., Harris, N.W., and Tindle, A.G., 1984. Trace element discrimination diagrams for the tectonic interpretation of granitic rocks. Journal of Petrology, 25: 956–983.

Pearce, J.A., and Peate, D.W., 1995. Tectonic implications of the composition of volcanic arc magmas. Annual Review of Earth and Planetary Sciences, 23: 251–285.

Petford, N., and Atherton, M., 1996. Na-rich partial melts from newly underplated basaltic crust: The Cordillera Blanca Batholith. Peru. Journal of Petrology, 37(6): 1491–1521.

Qin, J.F., Lai, S.C., Wang, J., and Li, Y.F., 2007. High-$Mg^{\#}$ adakitic tonalite from the Xichahe area, Southing Qinling orogenic belt (central China): Petrogenesis and geological implications. International Geology Review, 49: 1145–1158.

Rapp, R.P., and Watson, E.B., 1995. Dehydration melting of metabasalt at 8–32 kbar: Implications for continental growth and crust-mantle recycling. Journal of Petrology, 36(4): 891–931.

Rapp, R.P., Shimizu, N., Norman, M.D., and Applegate, G.S., 1999. Reaction between slabderived melts and peridotite in the mantle wedge: Experimental constraints at 3.8 GPa. Chemical Geology, 160: 335–356.

Schiotte, L., Compston, W., and Bridgwater, D., 1988. Late Archaean ages for the deposition of clastic sediments belonging to the Malene supracrustals, southern West Greenland: Evidence from an ion probe U-Pb zircon study. Earth and Planetary Science letters, 87: 45–58.

Sun, W., Li, S.G., Chen, Y.D., and Li, Y.J., 2002. Timing of synorogenic granitoids in the South Qinling, central China: Constraints on the evolution of the Qinling–Dabie orogenic belt. Journal of Geology, 110: 457–468.

Sun, S.S., and McDonough, W.F., 1989. Chemical and isotopic systematics of oceanic basalts: Implications for mantle composition and processes. In: Saunders, A.D., and Norry, M.J. (eds.), Magmatism in the Ocean Basins. Geological Society, London, Special Publications, 313–345.

Wan, L., Zeng, Z.X., Asimow, P.D., Zeng, Z.H., Peng, L.Z., Xu, D.L., Wei, Y.X., Liu, W., Lu, C.D., and Chang, W.Q., 2019. Mid-Neoproterozoic mafic rocks in the western Jiangnan orogen, South China: Intracontinental rifting or subduction? Journal of Asian Earth Science, 185: 104039.

Wang, J., and Li, Z.X., 2003. History of neoproterozoic rift basins in South China: Implications for Rodinia break-up. Precambrian Research, 122: 141–158.

Wang, X.C., Li, Z.X., Li, X.H., Li, Q.L., and Zhang, Q.R., 2011a. Geochemical and Hf-Nd isotope data of Nanhua rift sedimentary and volcaniclastic rocks indicate a Neoproterozoic continental flood basalt provenance. Lithos,

127: 427–440.
Wang, X.L., Jiang, S.Y., Dai, B.Z., Griffifin, W.L., Dai, M.N., and Yang, Y.H., 2011b. Age, geochemistry and tectonic setting of the Neoproterozoic (ca. 830 Ma) gabbros on the southern margin of the North China Craton. Precambrian Research, 190: 35–47.
Wang, H., Chen, L., Sun, Y., Liu, X., Xu, X., Chen, J., Zhang, H., and Diwu, C., 2007. ~4.1 Ga xenocrystal zircon from Ordovician volcanic rocks in western part of North Qinling orogenic belt. Chinese Science Bulletin, 52: 3002–3010.
Wang, X., Zhou, J., Qiu, J., and Gao, J., 2004. Comment on Neoproterozoic granitoids in South China: Crustal melting above a mantle plume at ca. 825 Ma? Precambrian Research, 132: 401–403.
Wang, Z.Q., Yan, Q.R., Yan, Z., Wang, T., Jiang, C.F., Gao, L.D., Li, Q.G., Chen, J.L., Zhang, Y.L., Liu, P., Xie, C.L., and Xiang, Z.J., 2009. New division of the main tectonic unites of the Qinling orogenic belt, central China. Acta Geologica Sinnca, 83: 1527–1546 (in Chinese with English abstract).
Wang, H., Li, Z.W., Liu, S.G., Ran, B., Song, J.M., Li, J.X., Ye, Y.H., and Li, N., 2020. Ediacaran extension along the northern margin of the Yangtze Platform, South China: Constraints from the lithofacies and geochemistry of the Doushantuo Formation. Marine and Petroleum Geology, 112: 104056.
Wang, R.R., Xu, Z.Q., and Santosh, M., 2019. Neoproterozoic magmatism in the northern margin of the Yangtze Block, China: Implications for slab rollback in a subduction-related setting. Precambrian Research, 327: 176–195.
Wang, Y.J., Zhang, Y.Z., Cawood, P.A., Zhou, Y.Z., Zhang, F.F., Yang, X., and Cui, X., 2019. Early Neoproterozoic assembly and subsequent rifting in South China: Revealed from mafic and ultramafic rocks, central Jiangnan Orogen. Precambrian Research, 331: 105367.
Wang, R.R., Xu, Z.Q., Santosh, M., Yao, Y., Gao, L.E., and Liu, C.H., 2016. Late Neoproterozoic magmatism in South Qinling, central China: Geochemistry, zircon U-Pb-Lu-Hf isotopes and tectonic implications. Tectonophysics, 683: 43–61.
Wei, S.D., and Zhao, J.H., 2020. Neoproterozoic tourmaline-bearing peraluminous granitoids in the western Jiangnan Orogen, South China: Geochemistry, petrogenesis and tectonic implications. Precambrian Research, 347: 105831.
Whalen, J.B., Currie, K.L., and Chappell, B.W., 1987. A-type granites: Geochemical characteristics, discrimination and petrogenesis. Contributions to Mineralogy and Petrology, 95: 407–419.
Williams, I.S., and Claesson, S., 1987. Isotope evidence for the Precambrian province and Caledonian metamorphism of high grade paragneiss from the Seve Nappes, Scandinavian Caledonian. II, Ion microprobe zircon U-Th-Pb. Contributions to Mineralogy and Petrology, 97: 205–217.
Woodhead, J.D., Eggins, S.M., and Johnson, R.W., 1998. Magma genesis in the New Britain island arc: Further insights into melting and mass transfer processes. Journal of Petrology, 39: 1641–1668.
Wu, F.F., Wang, Z.Q., Wang, T., Yan, Z., and Chen, L., 2012. SHRIMP zircons U-Pb ages and geochemical characteristics of the Banbanshan K-feldspar granite in Shanyang, Southern Qinling orogenic belt. Journal of Mineralogical and Petrological Sciences, 32: 63–73 (in Chinese with English abstract).
Wu, Y., and Zheng, Y., 2013. Tectonic evolution of a composite collision orogen: An overview on the Qinling–Tongbai–Hong'an–Dabie–Sulu orogenic belt in central China. Gondwana Research, 23: 1402–1428.
Xia, L.Q., Xia, Z.C., Li, X.M., Ma, Z.P., and Xu, X.Y., 2008. Petrogenesis of the Yaolinghe Group, Yunxi Group, Wudangshan Group volcanic rocks and basic dyke swarms from eastern part of the South Qinling Mountains. Northwestern Geology, 41(3): 1–29 (in Chinese with English abstract).
Xiang, Z.J., Yan, Q.R., White, J.D.L., Song, B., and Wang, Z.Q., 2015. Geochemical constraints on the provenance and depositional setting of Neoproterozoic volcaniclastic rocks on the northern margin of the Yangtze Block, China: Implications for the tectonic evolution of the northern margin of the Yangtze Block. Precambrian Research, 164: 140–155.
Xue, H.M., Ma, F., and Song, Y.Q., 2011. Geochemistry and SHRIMP zircon U-Pb data of Neoproterozoic meta-magamtism rocks in the Suizhou–Zaoyang area, northern margin of the Yangtze Craton, central China. Acta Petrologica Sinica, 27: 1116–1130 (in Chinese with English abstract).
Yan, Z., Wang, Z.Q., Chen, J.L., Yan, Q.R., and Wang, T., 2010. Detrital record of Neoproterozoic arc-magmatism along the NW margin of the Yangtze Block, China: U-Pb geochronology and petrography of sandstones. Journal of Asian Earth Science, 37: 322–334.
Yang, J.H., Wu, F.Y., Wilde, S.A., and Liu, X.M., 2007. Petrogenesis of Late Triassic granitoids and their enclaves with implications for post-collisional lithospheric thinning of the Liaodong Peninsula, North China Craton. Chemical Geology, 242: 155–175.
Yang, Z.Y., Sun, Z.M., Yang, T.S., and Pei, J.L., 2004. A long connection (750–380 Ma) between South China and Australia: Paleomagnetic constraints. Earth and Planetary Science Letters, 220: 423–434.
Yang, P.T., Liu, S.W., Li, Q.G., Wang, Z.Q., Wang, W., and Bai, X., 2012. Emplacing age of the Tiewadian pluton in the South Qinling tectonic belt and its geological implications. Acta Geologica Sinica, 86(9):1525–1540 (in Chinese with English abstract).
Yao, J.L., Cawood, P.A., Shu, L.S., and Zhao, G.C., 2019. Jiangnan Orogen, South China: A ~970–820 Ma Rodinia margin accretionary belt. Earth Science Review, 196: 102872.
Zhang, G.W., Meng, Q.R., and Lai, S.C., 1995. Tectonics and structure of the Qinling orogenic belt. Science in China (Series B), 38: 1379–1394.
Zhang, G.W., Zhang, B.R., Yuan, X.C., and Xiao, Q.H., 2001. Qinling Orogenic Belt and Continental Dynamics. Beijing: Science Press, 1–855.
Zhang, J., Zhang, H.F., and Li, L., 2018. Neoproterozoic tectonic transition in the South Qinling belt: New constraints from geochemistry and zircon U-Pb-Hf isotopes of diorites from the Douling Complex. Precambrian Research, 306: 112–128.
Zhang, J.B., Liu, Y.X., Ding, X.Z., Zhang, H., and Zhang, C.H., 2020. Post-collisional ca. 800 Ma A-type felsic volcanic rocks in the eastern Jiangnan orogen, South China. Journal of Asian Earth Sciences, 203: 104567.
Zhang, S.B., and Zheng, Y.F., 2013. Formation and evolution of Precambrian continental lithosphere in South China. Gondwana Research, 23: 1241–1260.
Zhang, C.L., Li, M., Wang, T., Yuan, H.L., Yan, Y.X., Liu, X.M., Wang, J.Q., and Liu, Y., 2004. U-Pb zircon geochronology and geochemistry of granitoids in the Douling Group in the eastern Qinling. Acta Geologica Sinica (English Edition), 78: 83–95.
Zhao, J.H., and Zhou, M.F., 2009. Secular evolution of the Neoproterozoic lithospheric mantle underneath the northern margin of the Yangtze Block, South China. Lithos, 107: 152–168.
Zhao, G.C., and Cawood, P.A., 2012. Precambrian Geology of China. Precambrian Research, 222–223: 13–54.
Zhao, J.H., Li, Q.W., Liu, H., and Wang, W., 2018. Neoproterozoic magmatism in the western and northern margins of the Yangtze Block (South China) controlled by slab subduction and subductiontransform-edge-propagator. Earth-Science Review, 187: 1–18.
Zhao, J.H., Zhou, M.F., Zheng, J.P., and Fang, S.M., 2010. Neoproterozoic crustal growth and reworking of the Northwestern Yangtze Block: Constraints from the Xixiang dioritic intrusion, South China. Lithos, 120: 439–452.
Zhao, J.H., Zhou, M.F., Yan, D.P., Zheng, J.P., and Li, J.W., 2011. Reappraisal of the ages of Neoproterozoic strata in South China: No connection with the Grenvillian orogeny. Geology, 39: 299–302.
Zhao, J.H., and Zhou, M.F., 2008. Neoproterozoic adakitic plutons in the northern margin of the Yangtze Block, China: Partial melting of a thickened lower crust and implications for secular crustal evolution. Lithos, 104: 231–248.
Zheng, Y., Zhao, Z., Wu, Y., Zhang, S., Liu, X., and Wu, F.,

2006. Zircon U-Pb age, Hf and O isotope constraints on protolith origin of ultrahigh-pressure eclogite and gneiss in the Dabie orogen. Chemical Geology, 231: 135–158.
Zheng, Y.F., Wu, Y.B., Chen, F.K., Gong, B., Li, L., and Zhao, Z.F., 2004. Zircon U-Pb and oxygen isotope evidence for a large-scale ^{18}O depletion event in igneous rocks during the Neoproterozoic. Geochimica et Cosmochimica Acta, 68: 4145–4165.
Zhou, J.B., Li, X.H., Ge, W.C., and Li, Z.X., 2007. Age and origin of middle Neoproterozoic mafic magmatism in southern Yangtze Block and relevance to the break-up of Rodinia. Gondwana Research, 12: 184–197.
Zhou, M.F., Kennedy, A.K., Sun, M., Malpas, J., and Lesher, C.M., 2002a. Neoproterozoic arcrelated mafific intrusions in the northern margin of South China: Implications for accretion of Rodinia. Journal of Geology, 110: 611–618.
Zhou, M.F., Yan, D.P., Kennedy, A.K., Li, Y.Q., and Ding, J., 2002b. SHRIMP zircon geochronological and geochemical evidence for Neoproterozoic arc-related magmatism along the western margin of the Yangtze Block, South China. Earth and Planetary Science Letters, 196: 51–67.
Zhu, X.Y., Chen, F.K., Liu, B.X., Zhang, H., and Zhai, M.G., 2014a. Geochemistry and zircon ages of mafic dikes in the South Qinling, central China: Evidence for late Neoproterozoic continental rifting in the northern Yangtze block. International Journal of Earth Sciences, 104: 27–44.
Zhu, X.Y., Chen, F.K., Nie, H., Siebel, W., Yang, Y.Z., Xue, Y.Y., and Zhai, M.G., 2014b. Neoproterozoic tectonic evolution of South Qinling, China: Evidence from zircon ages and geochemistry of the Yaolinghe volcanic rocks. Precambrian Research, 245: 115–130.
Zhu, X.Y., Chen, F.K., Wang, W., Pham, T.H., Wang, F., and Zhang, F.Q., 2008. Zircon U-Pb ages of volcanic and sedimentary rocks of the Wudang Group in the Qinling orogenic belt within eastern Henan Province. Acta Geoscience Sinica, 29: 817–829 (in Chinese with English abstract).

About the first author

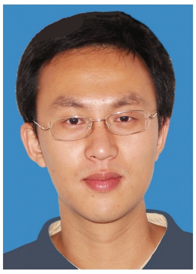

WANG Shuo, male, born in 1984 in Changchun, Jilin Province; doctor; graduated from Jilin University; associate professor of the School of Earth Science and Resources, Chang'an University. He is now interested in the study of regional mineralization. E-mail: iamsure1984@163.com.

About the corresponding author

LIU Yunhua, male, born in 1965 in Meishan, Sichuan Province; Ph.D. in geology; graduated from Jilin University; professor of the School of Earth Science and Resources, Chang'an University. He is now interested in the study of tectonic evolution and mineralization. E-mail: zyyhliu@chd.edu.cn.